Materials Research Proceedings 41 (2024) 771-780 https://doi.org/10.21741/9781644903131-85

Numerical simulation of the extrusion process with different FEM code approaches: analysis of thermal field, profile speed, defects evolution, and microstructure of hollow tubes

PELACCIA Riccardo[1,a *], NEGOZIO Marco[2,b], DI DONATO Sara[3,c], REGGIANI Barbara [1,4,d], DONATI Lorenzo[3,e]

[1]DISMI Department of Sciences and Methods for Engineering, University of Modena and Reggio Emilia, Via Amendola 2, 42122, Reggio Emilia, Italy

[2]Department of Engineering and Architecture, University of Parma, Parco Area delle Scienze, 181/A, 43124 Parma, Italy

[3]DIN Department of Industrial Engineering, University of Bologna, Viale Risorgimento 2, 40136, Bologna, Italy

[4]INTERMECH, University of Modena and Reggio Emilia, Italy

[a]riccardo.pelaccia@unimore.it, [b]marco.negozio@unipr.it, [c]sara.didonato2@unibo.it, [d]barbara.reggiani@unimore.it, [e]l.donati@unibo.it

Keywords: Extrusion, Process Monitoring, Defect Analysis, Microstructure, FEM Validation

Abstract. Over the years, the utilization of FEM numerical simulation has become a valuable tool for both die makers and extruders. To assess the evolution of FEM codes in terms of problem-solving potentiality, accuracy, as well as reduction of computational time, the 'ICEB - International Conference on Extrusion and Benchmark' conference series was established. The participants, who are unaware of the experimental outputs in advance, share with the organizers their numerical results to be compared with the actual experimental data. Analysis and discussion of the results during the conference allows users to check if their simulation settings are adequate to replicate the problems, and software house to verify the sensitivity of their solving methods. For the ICEB 2023, hollow tube-shaped profiles in AA6082 were extruded by varying the nitrogen flow rate and the quenching conditions. The experimental-numerical comparison was assessed in terms of press load, profile speeds, profile and die temperatures, defects evolution, nitrogen cooling efficiency, and the profiles' microstructure.

Introduction

The 'ICEB - International Conference on Extrusion and Benchmark' conference series have been organized since 2007, not only to test the potentiality of the numerical tools, but also to propose interesting challenges and to improve the community's knowledge in the field of the extrusion process [1]. Over the years, the involvement of experts and not from different areas and backgrounds (FEM users, extruders, die makers, researchers, software houses…) has helped to create a specific conference on the extrusion process where discuss captivating challenges, understand the needs of the industrial framework, and verify the progress of FEM simulations for the process optimization. Notably, the organizers prepare and carry out the experimental campaign in collaboration with selected extruders and die makers: the die and profile geometry are selected to evidence problematics and challenges in terms of profile quality, die resistances, and defects as well as in terms of reliability of the numerical models. All necessary input data are shared with the participants, who have to simulate the case study by using the software they prefer, but without knowing the experimental results.

During the conference, the organizers compare the numerical results of the participants with the experimental ones, showing the achievements and the limits/challenges of the state of art [1-2].
In this context, the present work summarized the main outcomes obtained during the Extrusion Benchmark 2023, discussing the numerical results of the participants, and comparing them with the experimental outputs. Within the first six editions, in order to provide an even point of comparison between experiments and simulations, experimental trials were focused on critical aspects of the process: in 2007 different pocket design and profile thickness were tested finding that the slowing effect of the conical pocket can be more determining respect the profile thickness in terms of profile exiting velocities [3]; in 2009 two U-shape profiles were produced using different supporting legs to assess the die deformations induced by the design [4]; in 2011 different strategies for port-hole balancing were used for hollow profiles extrusion, evaluating the die deflections and the seam weld quality for the scientific case study [5], while a remarkable outcome of the industrial one was the decrease in profile temperature of 20°C using the die nitrogen cooling [6]; in 2013 the investigations were aimed at predicting the effects of mandrel deflection [7]; in 2015 the effect of bearing length and shape (straight, chocked or relieved) was examined [8-9]; while in 2017 the die design allowed mandrels shift during the process in order to verify profile distortions respect to nominal dimensions in addition to position of seam welds, microstructure size and charge welds evolution [10].

Following the same trend, for the Extrusion Benchmark 2023 a porthole die for hollow profile extrusion was designed with three tube-shaped openings (Fig. 1). The material flow within the tooling set was different for the 3 profiles (Fig. 2) with the aim to generate high velocity deviations at the exit. The experimental campaign involved the extrusion of fifteen AA6082 billets varying the nitrogen flow rate (0% or 100% valve opened) and the quenching conditions (air or water quenching) intending to evaluate the trend of the thermal field in both uncooled and cooled conditions as well as to assess the impact of quenching on the grain size evolution. The experimental outputs collected to provide a reliable comparison of FEM results were: press load, profile speeds, profile temperatures, die temperatures in eleven different locations, seam welds quality, charge welds and skin defect evolution, nitrogen cooling efficiency, and the microstructure size for both air and water quenched profiles.

Experimental setting

Fig. 3 schematizes the experimental trials: the first five billets were extruded without the nitrogen cooling and using only the air quenching; the subsequent four billets using the nitrogen cooling with the valve fully opened; from the tenth to the twelfth extrusion the water quenching was enabled by keeping the nitrogen cooling system active; the last three extrusion were performed maintaining only the water quenching active. The extrusion speed was set constant at a value of 4.4 mm/s as suggested by the extruder (Metra SpA, plant in Rodengo Saiano, Brescia, IT). Fig. 3 also reports indications about the profile selected for the defects analysis (charge welds and billet skin) and for the microstructure assessment. The tooling set and the profile geometries were designed in collaboration with Almax Mori, Rovereto, TN. Three identical tube-shaped profiles (external diameter of 40 mm, thickness of 4 mm) were generated from the die set (Fig. 1), however, the three openings had differences (Fig. 2) in the ports' geometry (i.e. cylindrical or conical ports) and the bearings' surface (bearing lengths and radii) to induce at the exit high velocity deviations and consequently different strains, strain rates and temperatures in the tubes. The cooling channel was realized on the backer surface in contact with the die, and the cooling path, that surrounds the profile exits, is shown in Fig. 1c. Fig. 4 reports the location of the eleven thermocouples used to monitor the thermal field of the tooling set, while a contactless pyrometer (1500 mm far from the bolster exit face) was used to register the temperature of profile 1. Table 1 summarizes the main input data shared with the participants, while all additional information (e.g. geometry CAD files) can be asked to benchmark organizers (iceb.din@unibo.it).

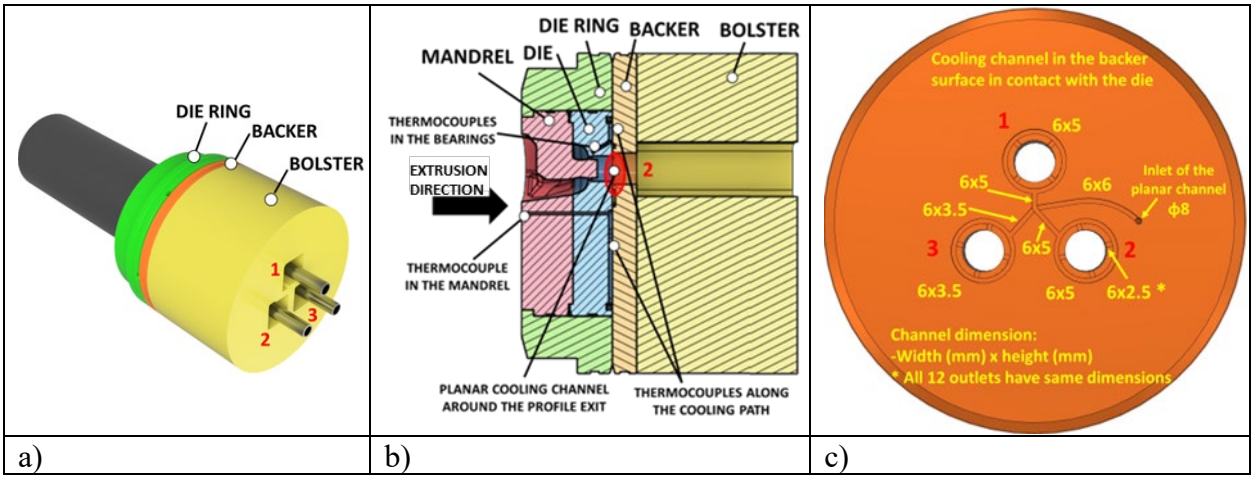

Fig. 1 ICEB 2023 case study: a) Rendering of the tools set-up, b) Tooling set composition, c) Cooling path.

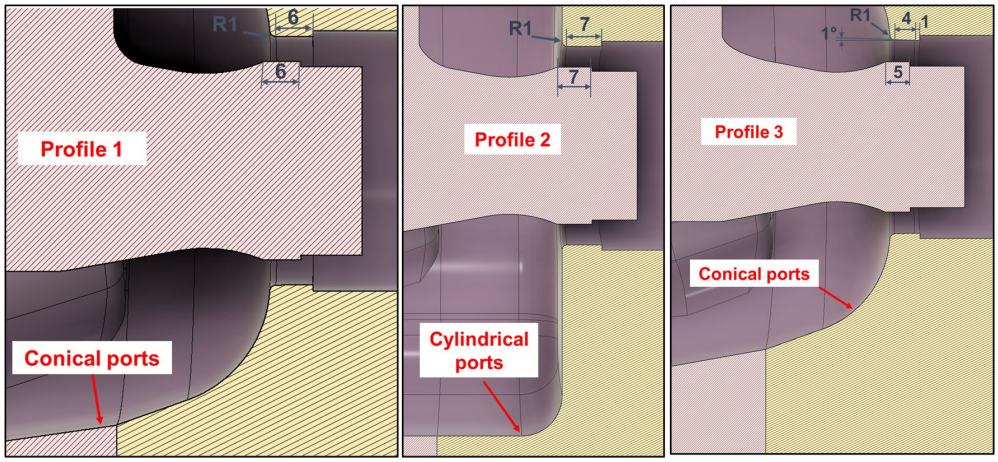

Fig. 2 Details of ports and bearings geometry for the three openings.

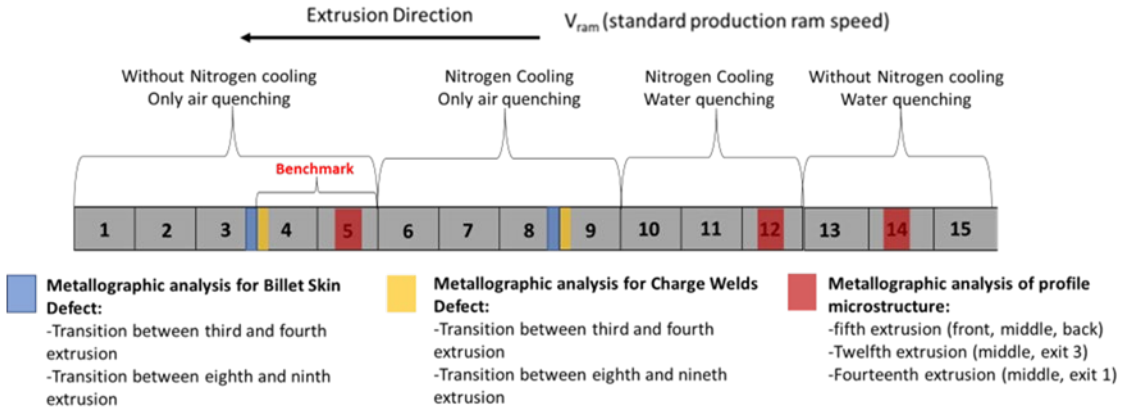

Fig. 3 Selected Design of Experiment (DOE) for Extrusion Benchmark 2023.

The requests for participants, which will be partly analyzed and discussed in the subsequent section, are reported:

Mandatory (on billet 4):

- Predicted press load; Profiles exit speeds; Profiles exit temperatures; Die temperatures in the eleven locations; Position of seam welds within the profiles.

Optional 1:

- Charge welds and skin defect evolution (billets 3-4 transition); Grain size with air quenching (billet 4 or 5); Grain size with water quenching (billet 14); Quality of the seam welds (billet 4).

Optional 2 (billet 11 with nitrogen cooling):

- Profiles exit temperature; Die temperatures in the eleven locations.

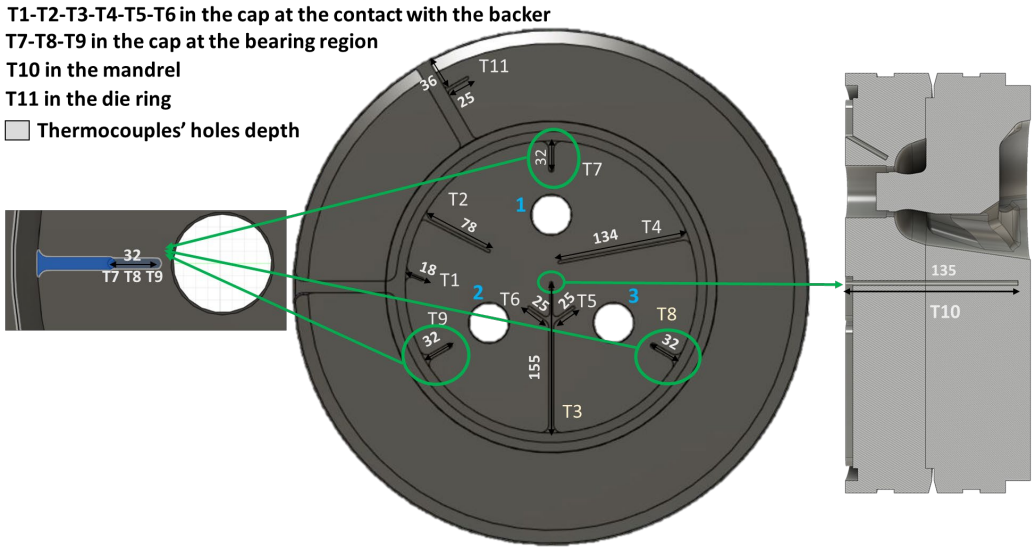

Fig. 4 Thermocouples' location within the tooling set.

Table 1 Process parameters and input data for participants

Process Parameter	Value
Profile alloy	AA6082 flow stress data in [11]
Billet/Container diameter	279 / 286 [mm]
Billet length	680 [mm]
Billet rest	30 [mm]
Skin layer thickness	0.3 [mm]
Ram speed -all tested conditions-	4.4 [mm/s]
Max press load	4000 [ton] / 40 [MN]
Ram/Container Temperature	350 / (390-425) (ram-die) [°C]
Pre-heating Billet/Die Temperature	440 (no taper) / 480 [°C]
Pyrometer distance from bolster surface	1500 [mm]
Water/air spray quenching box distance from bolster surface	2500 [mm]
Water/air spray quenching box length	4800 [mm]
Decrease of profile temperature (air/water quenching)	1 / 100 [°C/sec]
Initial average grain size	115 [µm]
Nitrogen Inlet Temperature	-196 [°C]
Nitrogen Inlet Pressure	3 [bars]
Nitrogen Inlet Tube Diameter (internal)	5,5 [mm]

Participants results: Experimental-numerical comparison

Twelve companies attended the Extrusion Benchmark 2023, but only four of them as active participants with their simulations: Hydro Innovation and Technology as research group, extruder and user of Qform UK software, Micas Simulations Limited as software house of Qform UK; Altair as software house of HyperXtrude; Almax Mori as die maker and user of HyperXtrude software. During the presentation and the discussion of the results, the four participants are

indicated randomly with the code from P1 to P4 as requested by themselves. However, the code always identifies the same participant.

Predicted Press Load. The experimental extrusion load was compared with those predicted by the participants for the fourth extrusion (steady-state uncooled condition). High accuracy of the numerical predictions was obtained with an average error below 10% with respect to the experimental maximum value of 36.1 MN.

Profile Exit Speeds. During the first run, before the use of the puller, the velocity of profile 2 was qualitatively 50% higher than the other two profiles. Then, despite the application of a tensile force of 3500 N, profile 2 continued to flow through the puller at a higher speed. In Table 2 the experimental velocity of profiles 1 and 3 was the same as the puller (avg. speed of 195 mm/s), while for profile 2, the average speed of 225 mm/s (15% higher than the puller one) was obtained by calculating the difference in terms of extrudates length at the end of the extrusion. In this case, the bearings optimization could be not enough to easily compensate for the speed differences generated by a conical port design (Fig. 2). Indeed, the experimental evidence demonstrated that the speed disparity between profile 3 and profile 1 (both extruded with conical ports) was relatively minimal and negligible without and with the puller, respectively, despite variations in bearing configuration (choke for profile 3, 1 mm higher bearing length for profile 1). Furthermore, despite profile 2 having a 1 mm greater bearing length than profile 1, the former exhibited a significant faster flow due to the presence of cylindrical ports. The numerical results were aligned with the experimental evidence of the first run (no one simulated the presence of the puller), where profile 1 was faster than profile 3, remaining profile 2 the fastest one.

Table 2 Profile exit speeds: Experimental-Numerical comparison (billet 4)

Profile exit speed / Billet 4	**Profile 1 [mm/s]**	**Profile 2 [mm/s]**	**Profile 3 [mm/s]**
Experimental	195	225	195
P1	213 (Num Err. +9.2%)	254 (Num Err. +12.8%)	141 (Num Err. -27.7%)
P2	183 (Num Err. -6.2%)	251 (Num Err. +11.5%)	176 (Num Err. -9.7%)
P3	183 (Num Err. -6.2%)	261 (Num Err. +16%)	161 (Num Err. -17.4%)
P4	184 (Num Err. -5.7%)	245 (Num Err. +8.9%)	160 (Num Err. -17.9%)

Profiles exit temperatures. The contactless pyrometer only registered the exit profile temperature of profile 1 that, during the fourth and the fifth runs, had stabilized at around 560 °C. In this case, the numerical results of the participants differed from each other due to the selection of dissimilar heat exchange with air. Indeed, despite all participants obtaining profile temperatures in the range of 550-570 °C near the bearings, the differences were more marked at the location of the pyrometer also among users of the same software: 570°C, 536°C, 495°C, and 520°C was predicted by P1, P2, P3, and P4, respectively. Therefore, P1 better predicted the low heat exchange with air (num. err. +1.8%), while other participants overestimated its cooling efficiency (max err. of -12.3% for P3). The exit profile temperature plays an important role in the prediction of the microstructure [12-14], therefore also the proper calibration of the thermal boundary conditions "downstream of the process" is not to be underestimated.

Die temperatures in the eleven locations. Fig. 5 reports the thermocouples' temperature recorded during the steady state uncooled condition (billet 4). The thermocouples T4-T6 nearby the profiles' exit recorded a maximum value of about 444 °C. T1 and T2 nearby the inlet channel marked 361°C and 406°C, respectively. T9 (bearings exit 2) indicated the value of 490 °C; T8 (bearings exit 3) only 445 °C, while T7 (bearings exit 1) recorded an intermediate value of 473 °C. As expected, the highest temperature of 535 °C was observed in T10 (mandrel) and the lowest one of about 295°C in T11 (die ring). Unfortunately, T7-T9 positions were not close enough to capture the real bearings temperature which should be very similar to the profile temperature (560 °C) [2].

Moreover, T8 temperature was unexpectedly low if compared to T7 since profiles 1 and 3 had the same velocity (Table 2). Therefore, during the die loading, T8 had probably moved out of place.

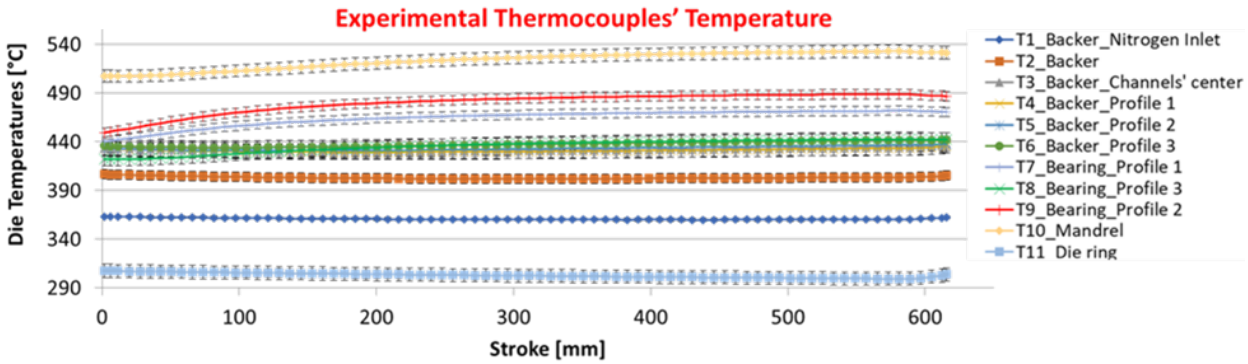

Fig. 5 Thermal history of the fourth extrusion

Table 3 Thermocouples' recordings: Experimental-Numerical comparison (billet 4)

Thermocouples' Temperature [°C]											
Billet 4	**T1**	**T2**	**T3**	**T4**	**T5**	**T6**	**T7**	**T8**	**T9**	**T10**	**T11**
Experimental	361	406	437	437	441	444	473	445	490	535	295
P1	365	390	405	405	407	409	496	497	499	492	334
P2	434	437	433	431	427	430	466	464	472	456	368
P3	374	396	408	406	408	412	482	461	494	452	310
P4	373	410	413	416	416	420	466	465	478	459	290

The numerical results (Table 3) were aligned with the experimental ones nearby the bearings (errors below 5% except in T8 for the above-mentioned reason), while average errors in the range of 5-10% were detected in the backer and the die ring (except for P2 with +25% in T11). A general temperature underestimation, in the range of 50-80 °C, was found only at T10 location (mandrel), however, the obtained results confirmed the improvement achieved over the years in terms of numerical thermal field prediction [2].

Extrusion Defects. The assessment of charge welds and billet skin defects involved the etching of the profile, the acquisition and the analysis of the images. All the analyzed profiles showed no evidence of billet skin contamination. Fig. 6b reports the evolution of charge welds for profile 1 in the transition between billets 3-4. The experimental trend for profile 2 was not analyzed due to the presence of the PCG (Peripheral Coarse Grain, Fig. 6c), which avoided precisely delineating the start and end points of the defect. For profiles 1 and 3, defects appeared within the range of +750-800 mm from the stopmark, followed by a complete replacement of the old billet material in the range of +2100-2200 mm (Fig. 6b). The numerical predictions underline the concrete possibility to optimize the scrap during the die design phase. Indeed, even if P4 greatly overestimated the start point of the charge welds with respect to the other participants, the end of the defect, and consequently, the distance from the stopmark to be scrapped was well predicted by everyone (max. err. of +10% for P4).

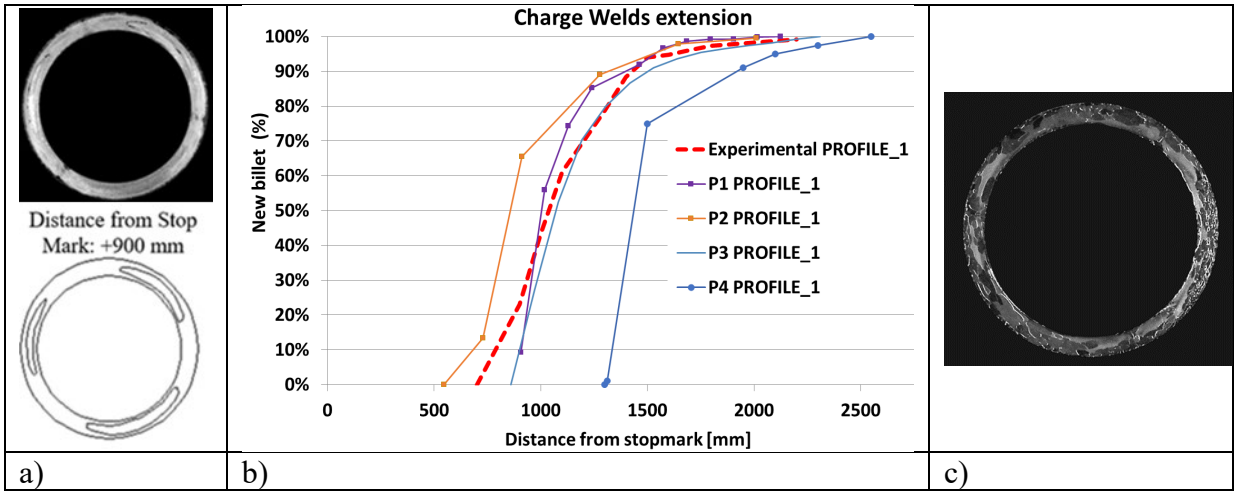

Fig. 6 Charge welds evolution for transitions between billets 3-4: a) Example of image analysis after etching, b) Experimental-Numerical comparison for the Profile 1, c) PCG layer in Profile 2 avoids evaluating the charge evolution

Seam Weld Quality. The numerical prediction of the seam weld quality established if a good welding is obtained, evaluating the material conditions (strain, strain rate, and temperature) within the welding chamber during the joint formation. The criteria proposed within the software differ from each other, however, all numerical results predicted qualitatively welding with good strength. For the characterization of the seam weld quality, bulge test was selected [15] where, thanks to the pressure of rubber plug on the inside wall of the profile, a biaxial tensile stress is generated leading the tube to fracture in the proximity of the seam welds. Therefore, the quantitative comparison between the numerical welding criteria and the experimental outputs in terms of load and hoop strain at fracture is not possible. The hoop strain at fracture was estimated as the natural logarithmic ratio between the final and the initial tube circumferences. Profile 1, 2, and 3 presented average values of 0.13, 0.08, and 0.14, respectively. Moreover, the peak load at fracture follows the same trend with average values of 56.1 kN, 51.5 kN, and 57.6 kN, respectively. The results of the experimental investigation clearly indicate that profile 3 demonstrates the highest level of deformability, as evidenced by both the hoop strain and peak load measurements. Profile 1 follows closely in terms of deformability, whereas profile 2 exhibits lower values due to the presence of coarser grain structure, as discussed in the microstructure section.

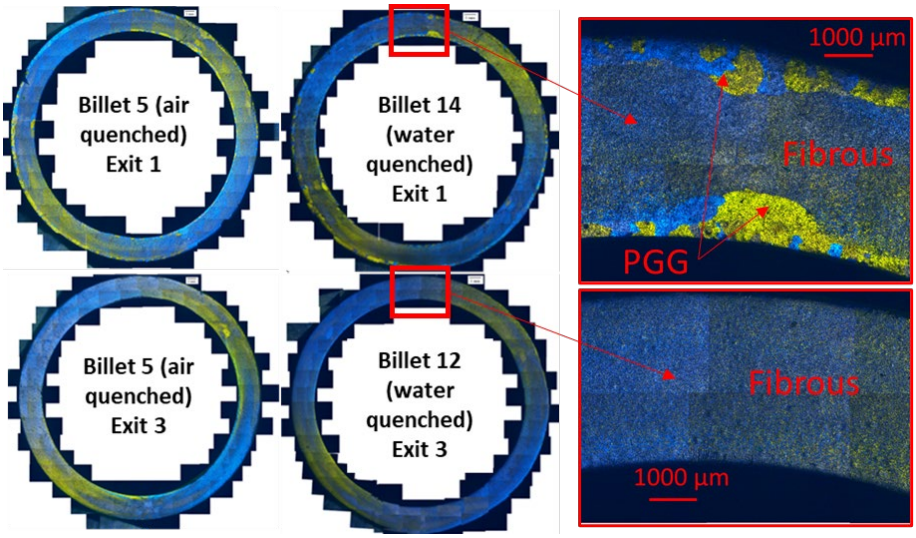

Fig. 7 Comparison between air and water quenching in terms of obtained grain size

Microstructure. Specimens extracted from the middle of the extruded profiles were analyzed in terms of microstructure evolution. The image was acquired by using polarized light microscopy of the samples anodized (40 V dc, 4 min) with Barker's reagent (15 mL HBF4, 750 mL H2O). In order to measure the recrystallization layer on both the internal and external surfaces, measurements every 30° of the circumference were acquired (average values are summarized in Table 4). In Fig. 7, the comparison of microstructures obtained with air quenching and with water quenching are reported for profiles 1 and 3. The microstructure of profile 1 exhibits a fibrous grain structure with a thin PCG layer on the internal and external surfaces, while profile 3 shows a completely fibrous microstructure. In contrast, as previously shown in Fig. 6c, profile 2 presents a very large PCG thickness, both internally and externally, caused by the higher exit speed of the profile. As depicted in Fig. 7, the impact of water quenching on the evolution of grain size was found to be negligible. This suggests that the formation of PCG occurred within a shorter timeframe than the interval between the profile exit from the bearings and its arrival at the water quenching box. Furthermore, the obtained results emphasized the strong dependency between PCG formation and material conditions such as strain, strain rate, and temperature, as proved by the significant variations in microstructure observed between profiles 2 (with thick PCG layers) and 3 (with an absence of PCG). All participants (except for P4 that did not perform this simulation) used models for dynamic recrystallization that do not take into account the PCG formation [12-14]. Therefore, the numerical outputs showed large discrepancies with the experimental results, predicting (all participants in a similar way) a grain size within the range 5-80 [μm] with the absence of PCG. Numerical findings underline that the prediction of the microstructure evolution, especially for complex case studies, still remains a challenge for the industrial scene.

Table 4 Experimental-Numerical comparison in terms of obtained grain size (billet 5)

Billet 5	Avg Int PCG layer [μm]	Avg Ext PCG Layer [μm]	Grain size range [μm]	
Exp Exit 1	201	523	5-30 Fibrous	131-832 PCG
Exp Exit 2	485	1154	5-30 Fibrous	142-1885 PCG
Exp Exit 3	0	0	5-30 Fibrous	0 PCG

Thermal field with nitrogen cooling. Fig. 8 exhibits the effect of nitrogen cooling on the exit profile temperature, the bearings, and the mandrel, comparing the results with the uncooled condition (billet 4 vs billet 11). In detail, the cooling efficiency on the profile surfaces was limited, causing a sole 10°C of change (from 560°C to 550°C for profile 1). The channel design promoted the nitrogen flow towards the exit of profile 3, a trend confirmed by the bearings temperatures, where the higher cooling effect was captured by T8 (exit 3, from 445 °C to 417 °C), while the lower one by T7 (exit 1, from 475°C to 463°C). The effect of nitrogen cooling was remarkable within the backer nearby the inlet channel and along the first part of the cooling path, registering in T1-T4 locations a general decrease of temperature in the range of 100-120 °C (table 5). In this case, the distance of the cooling channels from the bearings and the pressure drops induced by the design, which promoted an unbalanced nitrogen flow along the path, limited the effect of the cooling on the profile surface. Therefore, according to the state of art [2, 16-17], the experimental campaign showed the potentiality of the nitrogen cooling, but also the wide margins of improvement of the channels if designed with the support of advanced numerical tools. As previously given for the microstructure prediction, the numerical results of the participants can be improved. P4 did not simulate the process with cooling, both P2 and P3 used equivalent thermal boundary conditions along the path, while only P1 implemented the study of the nitrogen flow along the channel. All results showed a general overestimation of the cooling efficiency within the tooling set, especially along the cooling path (T1-T6), not properly catching the differences in

nitrogen flow rate towards the three exits of the profiles. The usage of equivalent heat transfer coefficients, if not properly calibrated, does not allow capturing the change in the heat transfer induced by the process settings and the channel design (pressure drops, nitrogen phase-change…). On the other hand, the FEM simulation of nitrogen flow can be inaccurate if the nitrogen gas formation generated by poorly designed solutions is not taken into account [16-17].

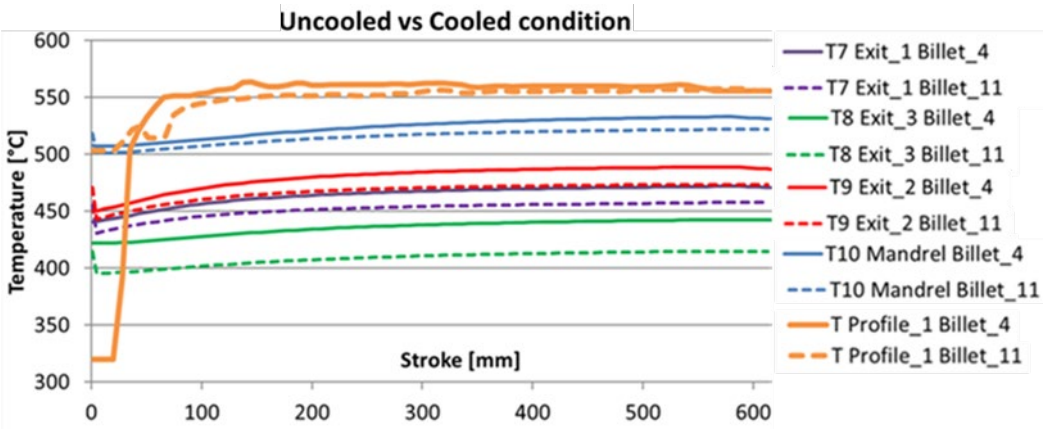

Fig. 8 Effect of nitrogen cooling on the profile temperature and the die thermal field

Table 5 Thermocouples' recordings: Experimental-Numerical comparison (billet 11)

Thermocouples' Temperature [°C]											
Billet 11	**T1**	**T2**	**T3**	**T4**	**T5**	**T6**	**T7**	**T8**	**T9**	**T10**	**T11**
Experimental	234	323	320	320	330	360	463	417	471	520	286
P1	148	192	117	129	138	196	476	468	477	491	334
P2	121	120	36	53	70	64	376	376	380	456	355
P3	113	189	208	226	236	271	467	440	474	451	301

Conclusions

In the Extrusion Benchmark 2023, the processing conditions for extruding three AA 6082 tubes were monitored and analyzed. The tests were performed on air and water quenched conditions and with the use or absence of liquid nitrogen cooling. In detail, the following experimental outputs were acquired for the comparison with the FEM results of the participants: press load, profile speed, profile temperatures, die temperatures in eleven different locations, microstructure size, charge welds and billet skin evolution, and seam weld quality with bulge test. Good accuracy of the numerical results was demonstrated in terms of press load, profile speed, and thermal field in uncooled conditions as well as in terms of evaluation of the extrusion scraps. A reliable forecast of the microstructure size and the effect of nitrogen cooling still remains a challenge.

Funding

National Recovery and Resilience Plan (NRRP), Mission 04 Component 2 Investment 1.5–NextGenerationEU, Call for tender n.3277 dated 30/12/2021 (Award Number: 0001052 dated 23/06/2022).

References

[1] B. Reggiani, L. Donati, L. Tomesani, ICEB - International conference on extrusion and benchmark, Light Metal Age 75 (5) (2017) 52 – 60.

[2] L. Donati, B. Reggiani, R. Pelaccia, M. Negozio, S. Di Donato, Advancements in extrusion and drawing: a review of the contributes by the ESAFORM community, Int. J. Mater. Form. 15 (2022) 41. https://doi.org/10.1007/s12289-022-01664-w

[3] M. Schikorra, L. Donati, L. Tomesani, A. E. Tekkaya, Extrusion Benchmark 2007 – Benchmark Experiments: Study on Material Flow Extrusion of a Flat Die, Key Eng. Mater. 367 (2008) 1-8. https://doi.org/10.4028/www.scientific.net/KEM.367.1

[4] D. Pietzka, et al., Extrusion Benchmark 2009 - Experimental analysis of deflection in extrusion dies. Key Eng. Mater. 424 (2010) 19 - 26. https://doi.org/10.4028/www.scientific.net/KEM.424.19

[5] A. Selvaggio, et al., Extrusion Benchmark 2011: Evaluation of different design strategies on process conditions, die deflection and seam weld quality in hollow profiles, Key Eng. Mater. 491 (2012) 1 – 10. https://doi.org/10.4028/www.scientific.net/KEM.491.1

[6] L. Donati, et al., Effect of liquid nitrogen die cooling on extrusion process conditions Key Eng. Mater. 491 (2012) 215 - 222. https://doi.org/10.4028/www.scientific.net/KEM.491.215

[7] A. Selvaggio, T. Kloppenborg, M. Schwane, et al., Extrusion Benchmark 2013 - Experimental Analysis of Mandrel Deflection, Local Temperature and Pressure in Extrusion Dies, Key Eng. Mater. 585 (2013) 13 – 22. https://doi.org/10.4028/www.scientific.net/KEM.585.13

[8] A. Selvaggio, L. Donati, et al., Scientific Benchmark 2015: Effect of choking and bearing length on metal flow balancing in extrusion dies, Mater. Today: Proc 2 (2015) 4704-4713. https://doi.org/10.1016/j.matpr.2015.10.003

[9] A. Gamberoni, L. Donati, et al., Industrial Benchmark 2015: process monitoring and analysis of hollow EN AW-6063 extruded profile, Mater. Today: Proc 2 (2015) 4714-4725. https://doi.org/10.1016/j.matpr.2015.10.004

[10] L. Donati L., A. Segatori et al., Extrusion Benchmark 2017: Effect of Die Design on Profile Quality and Distortions of Thin C-Shaped Hollow Profiles, Mater. Today: Proc 10 (2019) 171–184. https://doi.org/10.1016/j.matpr.2018.10.394

[11] R. Pelaccia, M. Negozio, et al. Extrusion Benchmark 2023: Effect of die design on profile speed, seam weld quality and microstructure of hollow tubes, Key Eng. Mater, under press.

[12] M. Negozio, et al., Numerical investigation of the surface recrystallization during the extrusion of a AA6082 aluminum alloy under different process conditions Int. J. Adv. Manuf. Technol. 129 (3-4) (2023) 1585-1599. https://doi.org/10.1007/s00170-023-12397-8

[13] T. Sheppard, Prediction of structure during shaped extrusion and subsequent static recrystallisation during the solution soaking operation, J. Mater. Process. Technol. 177 (1-3) (2006) 26-35. https://doi.org/10.1016/j.jmatprotec.2006.04.099

[14] M. Negozio, R. Pelaccia, L. Donati, et al., Simulation of the microstructure evolution during the extrusion of two industrial-scale AA6063 profiles, J. Manuf. Process. 99 (2023) 501-512. https://doi.org/10.1016/j.jmapro.2023.05.075

[15] B. Reggiani, L. Donati, Comparison of experimental methods to evaluate the seam welds quality in extruded profiles, Trans. Nonferrous Met. Soc China, 30 (3) (2020) 619-634. https://doi.org/10.1016/S1003-6326(20)65241-4

[16] R. Pelaccia, B. Reggiani, et al., Liquid nitrogen in the industrial practice of hot aluminium extrusion: experimental and numerical investigation, Int J Adv Manuf Technol. 119 (2022) 3141–3155. https://doi.org/10.1007/s00170-021-08422-3

[17] R. Pelaccia, P. E. Santangelo, A Homogeneous Flow Model for nitrogen cooling in the aluminum-alloy extrusion process, Int. J. Heat Mass Transf. 195 (2022) 123202. https://doi.org/10.1016/j.ijheatmasstransfer.2022.123202